Depressurization Amorphization of Single-Crystal Boron Carbide

X. Q. Yan,[1,2] Z. Tang,[3] L. Zhang,[1] J. J. Guo,[1] C. Q. Jin,[4] Y. Zhang,[2] T. Goto,[5] J. W. McCauley,[6] and M. W. Chen[1,5,*]

[1]*WPI Advanced Institute for Materials Research, Tohoku University, Sendai 980-8577, Japan*

[2]*Department of Materials Physics and Chemistry, University of Science & Technology Beijing, Beijing 100083, China*

[3]*Key Laboratory of Polar Materials and Devices, East China Normal University, Shanghai 200062, China*

[4]*Institute of Physics, Chinese Academy of Sciences, Beijing 100080, China*

[5]*Institute for Materials Research, Tohoku University, Sendai 980-8577, Japan*

[6]*U.S. Army Research Laboratory, Aberdeen Proving Ground, Maryland 21005, USA*

(Received 26 July 2008; published 20 February 2009)

We report depressurization amorphization of single-crystal boron carbide (B_4C) investigated by *in situ* high-pressure Raman spectroscopy. It was found that localized amorphization of B_4C takes place during unloading from high pressures, and nonhydrostatic stresses play a critical role in the high-pressure phase transition. First-principles molecular dynamics simulations reveal that the depressurization amorphization results from pressure-induced irreversible bending of C-B-C atomic chains cross-linking 12 atom icosahedra at the rhombohedral vertices.

DOI: 10.1103/PhysRevLett.102.075505 PACS numbers: 61.50.Ks, 07.35.+k, 78.30.−j, 82.40.Fp

Strong covalent solids generally possess very high strength and thereby are widely used as superhard materials for the applications where strength and hardness are critical. Nevertheless, the underlying mechanisms of deformation and failure of these materials subjected to high pressures are less known and have been a recent topic of intense discussion [1–7]. Boron carbide (B_4C) is one of the superhard materials and has been used as an armor ceramic because of its hardness combining with high Hugoniot elastic limit (HEL) and extremely low density [8]. Extensive shock loading tests have demonstrated that B_4C is effective for protection against high-pressure impact. However, when impact pressures are above ~20 GPa, an abrupt drop in shear strength occurs, leading to dynamic performance of B_4C much lower than that expected from its hardness and HEL [9–12]. High-resolution electron microscopy (HREM) of shock-loaded B_4C reveals that the anomalous shear softening is associated with shock-induced amorphization [3]. In addition to the shock loading experiments, the amorphization has also been observed in indented and mechanically scratched B_4C at high contact pressures but much low loading rates [13–16]. Therefore, the shear softening of B_4C is most likely associated with pressure-induced amorphization. It is thus expected that more controllable high-pressure diamond anvil cell (DAC) experiments may provide unique insights on the phase transition. A number of DAC experiments have been carried out with pressures up to ~50 GPa and, mysteriously, amorphous B_4C has not been found [17–19]. In this Letter, we report that the amorphization of B_4C in the form of nanosized bands takes place during unloading from high pressures, and nonhydrostatic stresses play a critical role in the high-pressure amorphization.

In this study, high pressures were generated using a piston-cylinder-type diamond anvil cell with a 350 μm culet. Samples with a size of ~30 μm in their longest dimension were cut from ~10 μm thick (223) B_4C single crystals [15]. The prepolished crystals were loaded into the DAC and placed with one face in contact with the diamond window for collecting Raman signals in backscattering geometry. Powdery B_4C and NaCl were used as pressure-transmitting media (PTM). The applied pressures were measured by both the ruby luminescence and diamond Raman scales. A Renishaw micro-Raman spectrometer with the excitation laser line at 514.5 nm was employed to characterize the structure of B_4C at high pressures. The structure evolution of pressurized B_4C was investigated by the first-principles molecular dynamics simulations based on the density functional theory within the generalized gradient approximation [20]. The microstructure of pressurized samples was characterized by a high-resolution electron microscope (HREM) with a field emission gun.

Figures 1(a) and 1(b) show Raman spectra of B_4C pressurized up to ~50 GPa and depressurized to ~1.1 GPa. In this experiment, the PTM is powdery NaCl that has much lower shear strength and can keep a good quasihydrostatic condition at high pressures. A number of Raman bands appears in the spectra, representing the complex atomic configurations of B_4C, i.e., 12 atom icosahedra at the rhombohedral vertices crosslinked by three-atom chains [21,22]. It has been demonstrated that amorphous B_4C has three characteristic Raman bands at ~1326, 1520, and 1810 cm^{-1} [13,15]. Because the frequency range of 1300–1500 cm^{-1} is covered by the strong scattering from the diamond window, the high-frequency region from 1500 to 2000 cm^{-1} was scanned to detect the amorphous band at ~1810 cm^{-1}. Although the changes in the positions and intensities of the Raman peaks can be readily observed with pressure increase and decrease, detectable amorphous B_4C corresponding to the Raman band

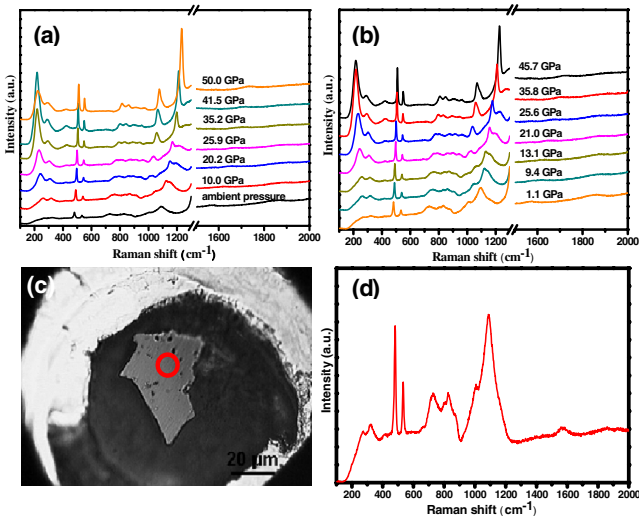

FIG. 1 (color online). High-pressure Raman spectra of single-crystal B_4C loaded in DAC with powdery NaCl as PTM. (a) Raman spectra of B_4C loaded from ambient pressure up to 50 GPa; (b) unloaded from 50 GPa to ~1.1 GPa; (c) pressurized B_4C crystal; and (d) Raman spectrum acquired from the marked region in (c).

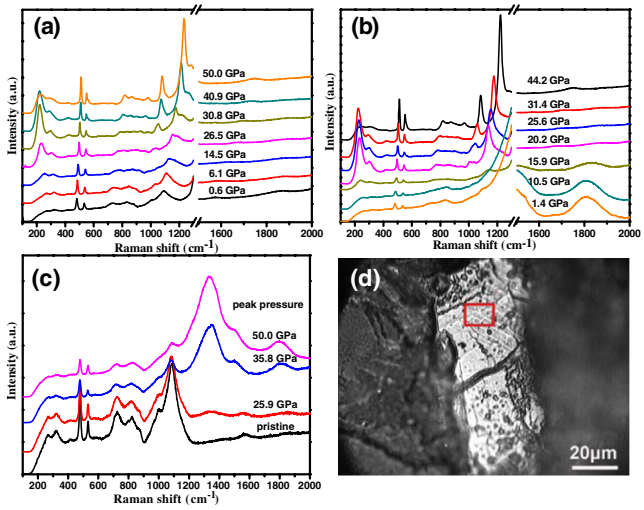

FIG. 2 (color online). High-pressure Raman spectra of single-crystal B_4C loaded in DAC with powdery B_4C as PTM. (a) Raman spectra of B_4C loaded from ambient up to 50 GPa, (b) unloaded from 50 GPa to ~1.4 GPa; and (c) Raman spectra of recovered B_4C pressurized to 25.9, 35.8, and 50 GPa. (d) Optical micrograph of the recovered sample pressurized to 50 GPa. Cracks and surface relief reveal that the crystal is loaded under a nonhydrostatic state. The Raman spectra shown in (c) are acquired from the region free of cracks, for example, the marked region in (d).

at ~1810 cm^{-1} has not been found during both pressurization and depressurization, which is consistent with previous high-pressure studies [17–19]. The obvious sharpening and intensity increasing of the 256 cm^{-1} and 1190 cm^{-1} bands at pressures above 20 GPa are mainly due to the resonant Raman scattering and polarization. Postmortem characterization of the pressurized B_4C crystals taken out from the DAC reveals that the sample remains perfect without visible surface relief and cracks [Fig. 1(c)], suggesting very good quasihydrostatic conditions during loading and unloading. Moreover, amorphous B_4C cannot be detected after the diamond window is removed [Fig. 1(d)].

To investigate the nonhydrostatic effect on elastic stability of B_4C at high pressures [2,4,23,24], hard and stiff B_4C powder was used to replace soft NaCl as the PTM. Figure 2(a) shows Raman spectra of single-crystal B_4C acquired with the loading pressures gradually increasing from the ambient up to ~50 GPa. Again, except the band intensity change caused by the resonant Raman scattering and polarization, the appearance of new peaks and disappearance of the crystalline peaks induced by phase transitions at high pressures have not been seen. In particular, detectable intensity change of Raman scattering at ~1810 cm^{-1} has not been found with the peak pressures loaded up to 50 GPa. To detect possible phase transitions during depressurization, *in situ* Raman characterization was performed when the applied pressures were gradually decreased from 50 to ~1.4 GPa [Fig. 2(b)]. The amorphous phase cannot be detected until the pressure is down to ~20 GPa. At ~15.9 GPa, the characteristic band of amorphous B_4C at ~1810 cm^{-1} emerges, and its intensity steadily increases with the decrease of the pressures to ~10 GPa [Fig. 2(b)]. The depressurization amorphization and the critical pressure, ~13–16 GPa, were reproduced by a number of tests with powdery B_4C as the PTM and without PTM. Postmortem Raman characterization shows that the amorphous phase produced by depressurization can be retained to ambient pressure, and all the three characteristic Raman bands of amorphous B_4C at 1326, 1520, and 1810 cm^{-1} can be detected after the diamond window is removed [Figs. 2(c) and 2(d)]. In addition to the critical pressure for the depressurization amorphization, there is also a threshold peak pressure for the amorphization, which is determined to be ~25 GPa. Below this value, the depressurization amorphization of B_4C cannot be detected by both *in situ* Raman spectroscopy and postmortem characterization. In the depressurization experiments, when the peak pressures are higher than the threshold value, the intensities of the amorphous B_4C peaks progressively increase with the increase of the peak pressures as shown in Fig. 2(c).

We noticed that the intensity of the amorphous B_4C Raman peaks varies with detected regions, implying that the distribution of amorphous B_4C is inhomogeneous. To verify the inhomogeneity, Raman maps of the amorphous B_4C bands were acquired from the recovered samples with the peak pressures of ~25.9, 35.8, and 50 GPa. The imaged regions are selected to be free of visible cracks [Figs. 3(a)–3(c)]. Evidently, it was observed that the amorphous phase with bright contrast in the maps [Figs. 3(d)–3(f)] is in the

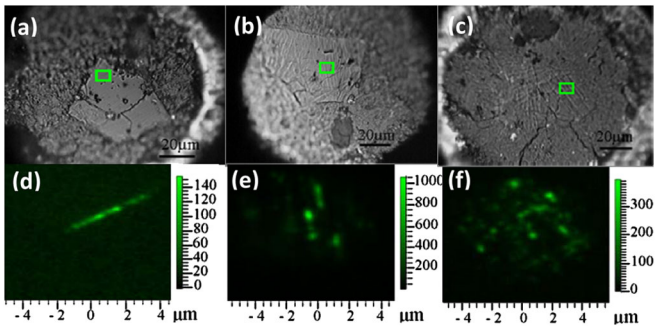

FIG. 3 (color online). Optical micrographs and Raman maps of depressurized single-crystal B_4C. (a) and (d) quenched from 25.9 GPa; (b) and (e) from 35.8 GPa; and (c) and (f) from 50 GPa. Raman maps taken from the rectangle regions in (a), (b), and (c) are imaged using amorphous peak at $\sim 1326\ cm^{-1}$.

form of narrow zones that are parallel to each other along a certain crystallographic plane. The density of the bright zones increases with the peak pressures, which strongly suggests that the amorphization of B_4C occurs by individual nucleation events, rather than the continuous growth of the existed amorphous zones. Comparing the optical micrographs with the Raman maps, one can find that the amorphous zones coincide with the surface rugosity. Since the initial surfaces of the single-crystal specimens are polished to be mirrorlike, it is believed that the surface rugosity is produced by high-pressure plastic deformation through the formation of amorphous zones driven by nonhydrostatic stresses. The localized amorphization is further confirmed by HREM of the recovered B_4C samples pressurized to $\sim$50 GPa without PTM. The pressurized single crystal was found to break into a number of small pieces. Shear bands can be observed in fragments with thin edges.

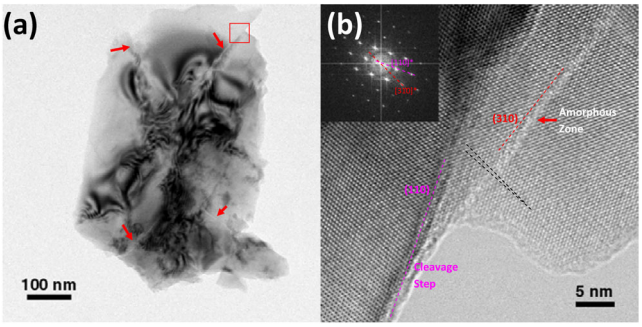

FIG. 4 (color online). Transmission electron microscopy of recovered B_4C with a peak pressure of $\sim$50 GPa. (a) A small fragment with shear bands (marked by arrowheads) and elastic Bragg contour patterns. (b) HREM micrograph of an amorphous band with a width of $\sim 1-2$ nm. This image is zoomed in from the marked region in Fig. 3(a) and taken along the $[001]^*$ zone direction of rhombohedral B_4C. The amorphous band is approximately parallel to a (310) plane whereas the cleavage facet is parallel to a (110) plane.

In the vicinity of the shear bands, strong Bragg contour patterns are visible [Fig. 4(a)], indicating large residual elastic strains. HREM reveals that amorphization takes place within the shear bands and the amorphous zones shown in Fig. 2 have an actual width of about 1–2 nm [Fig. 4(b)]. Dislocated lattices on both sides of the amorphous zone prove shear displacements along the band, indicating that the plastic deformation of B_4C at high pressures can be carried out by the amorphous zones. Moreover, conventional deformation defects, such as twins, stacking faults, and dislocations, that are frequently observed in shock-loaded ceramics [3,7] cannot be found.

The atomic origins of B_4C amorphization were theoretically investigated by first-principles MD simulations. Figure 5(a) presents the calculated volume compression of B_4C with the energetically most favorable polytype, i.e., $B_{11}Cp(C-B-C)$ [6,21], under hydrostatic pressures (squares). Continuous elastic deformation is observed over the entire simulated range from 0 to 60 GPa. As an example, Fig. 5(b) shows the atomic structures of B_4C at 0 and 47.6 GPa. These two configurations [**A** and **E** in Fig. 5(b)] are nearly identical except for the isotropic

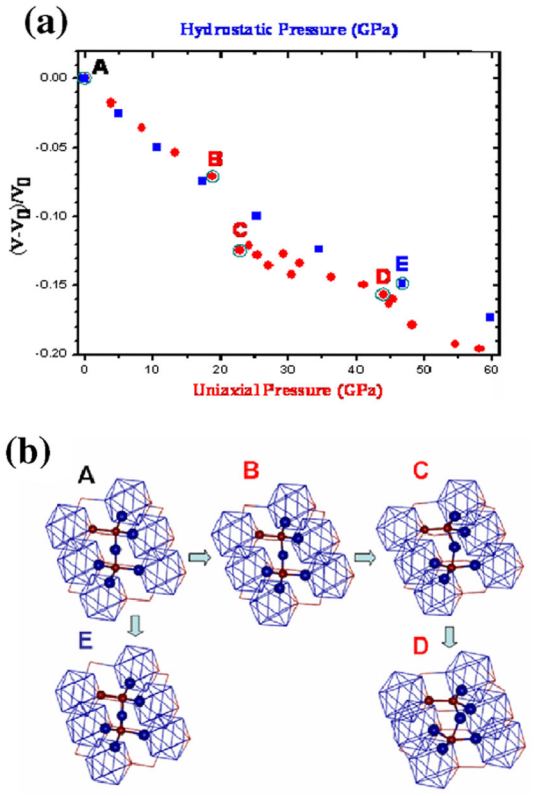

FIG. 5 (color online). First-principles simulations of the stabilization of B_4C under hydrostatic and uniaxial compression. (a) Compressed volumes vs pressures. The square data represent the volume change with hydrostatic pressure, and the circle data correspond to the volume change with uniaxial stress along the C-B-C atomic chain. (b) Atomic configurations of a B_4C unit cell at various pressures corresponding to the data points in (a).

volume shrinking induced by pressures, suggesting that the structural phase transition is absent with the hydrostatic pressures up to 60 GPa. However, structure destabilization of B_4C takes place with nonhydrostatic loading by compressing the system along the C-B-C atomic chain, followed by a cell-variable relaxation perpendicular to the chain. This chain direction has the largest Young's modulus and is thus the strongest orientation of B_4C [25]. The simulated volume compressions *versus* the uniaxial pressures [circles in Fig. 5(a)] shows that the system is elastically deformed up to 18.9 GPa. Further increasing the pressure to ~22.8 GPa leads to a discontinuous volume change, i.e., ~4% sudden volume reduction. The evolution of the atomic structures [**A**, **B**, and **C** presented in Fig. 5(b)] reveals that the discontinuous volume change corresponds to the bending of the C-B-C chain and the icosahedra at the rhombohedral vertices remain intact [26]. The bending angle becomes more visible with the increase of the uniaxial pressures [**D** in Fig. 5(b)]. When the bending angle is large enough, the middle boron atom in the three-atom chain is found to form new covalent bonds with the neighboring atoms in the icosahedra at the rhombohedral vertices. The new bonds prevent the recovery of the bended chain and result in irreversible structure change and distorted rhombohedral lattices with a high energy during unloading, which can trigger the collapse of the B_4C crystal structure and give rise to the unusual depressurization amorphization.

Depressurization amorphization has been observed in a number of materials and is generally related to metastable high-pressure phases [27,28]. However, the depressurization amorphization of B_4C shows an unusual manner that is caused by irreversible lattice distortion at high pressures. In general, localized phase transitions may originate from planar crystal defects [29]. However, these defects have not been observed in pressurized B_4C. The localized amorphization is most likely associated with the coexistence of abundant B_4C polytypes with different high-pressure stability [6]. Interestingly, the static properties of B_4C are fairly consistent with its dynamic performances [9–12]. The threshold pressure, 25.9 GPa, is reasonably close to the onset pressure (23.3 GPa) of localized amorphization at which 2–3 nm wide amorphous bands appear in ballistic B_4C fragments [3]. The destabilization pressure (18.9–22.8 GPa) suggested by the first-principles calculations is well consistent with the HEL (15–20 GPa) of B_4C. Moreover, the critical pressure (~13–16 GPa) for the depressurization amorphization is within the range of various reported values (10–15 GPa) of the loss in shear strength of B_4C loaded above the HEL [9,10]. Therefore, our quantitative high-pressure measurements provide compelling evidence that the amorphization of B_4C is responsible for the loss of the shear strength of B_4C at high impact pressures. The remarkable similarity in high-pressure properties implies the analogous deformation or damage mechanisms of B_4C subjected to both static and dynamic high pressures.

*Corresponding author: mwchen@imr.tohoku.ac.jp

[1] R. H. Telling, C. J. Pickard, M. C. Payne, and J. E. Field, Phys. Rev. Lett. **84**, 5160 (2000).
[2] H. Chacham and L. Kleinman, Phys. Rev. Lett. **85**, 4904 (2000).
[3] M. W. Chen, J. W. McCauley, and K. J. Hemker, Science **299**, 1563 (2003).
[4] F. Occelli, P. Loubeyre, and R. Letoullec, Nature Mater. **2**, 151 (2003).
[5] P. S. Branicio, R. K. Kalia, A. Nakano, and P. Vashishta, Phys. Rev. Lett. **96**, 065502 (2006).
[6] G. Fanchini, J. W. McCauley, and M. Chhowalla, Phys. Rev. Lett. **97**, 035502 (2006).
[7] M. W. Chen, J. W. McCauley, D. Dandekar, and N. K. Bourne, Nature Mater. **5**, 614 (2006).
[8] F. Thévenot, J. Eur. Ceram. Soc. **6**, 205 (1990).
[9] D. E. Grady, Sandia National Laboratories, Albuquerque, NM Report SAND 94-3266, 1995.
[10] D. P. Dandekar, Army Research Laboratory, Aberdeen Proving Ground, Aberdeen, MD, ARL-TR-2456 2001.
[11] T. Mashimo, M. Uchino, J. Appl. Phys. **81**, 7064 (1997); Y. Zhang *et al.*, J. Appl. Phys. **100**, 113536 (2006).
[12] T. J. Vogler, W. D.Reinhart, and L. C. Chhabildas, J. Appl. Phys. **95**, 4173 (2004).
[13] V. Domnich, Y. Gogotsi, M. Trenary, T. Tanaka, Appl. Phys. Lett. **81**, 3783 (2002).
[14] D. Ge, V. Domnich, T. Juliano, E. A. Stach, and Y. Gogotsi, Acta Mater. **52** 3921 (2004).
[15] X. Q. Yan, W. J. Li, T. Goto, M. W. Chen, Appl. Phys. Lett. **88**, 131905 (2006).
[16] M. W. Chen and J. W. McCauley, J. Appl. Phys. **100**, 123517 (2006).
[17] R. J. Nelmes *et al.*, Phys. Rev. Lett. **74**, 2268 (1995).
[18] M. H. Manghnani, Y. Wang, F. Li, P. Zinin, and W. Rafaniello, *Science and Technology of High Pressure* (Universities Press, Hyderabad, India, 2000), pp. 945–948.
[19] T. J. Holmquist and G. R. Johnson, J. Appl. Phys. **100**, 093525 (2006).
[20] W. Kohn and L. J. Sham, Phys. Rev. **140**, A1133 (1965).
[21] D. R. Tallant, T. L. Aselage, A. N. Campbell, and E. Emin, Phys. Rev. B **40**, 5649 (1989).
[22] R. Lazzari, N. Vast, J. M. Besson, S. Baroni, and A. Dal Corso, Phys. Rev. Lett. **83**, 3230 (1999).
[23] D. Machon *et al.*, Phys. Rev. B **68**, 144104 (2003).
[24] D. Machon, P. Bouvier, P. Tolédano, and H. P. Weber., J. Phys. Condens. Matter **18**, 3443 (2006).
[25] K. J. McClellan, F. Chu, and J. M. Roper, J. Mater. Sci. **36**, 3403 (2001).
[26] X. Blase, Philippe Gillet, A. San Miguel, and P. Mélinon, Phys. Rev. Lett. **92**, 215505 (2004).
[27] S. M. Sharma and S. K. Sikka, Prog. Mater. Sci. **40**, 1 (1996).
[28] P. Richet, Nature (London) **331**, 56 (1988).
[29] K. J. Kingma, C. Meade, R. J. Hemley, H. K. Mao, and D. R. Veblen, Science **259**, 666 (1993).